Improved urban heat island mitigation using bioclimatic redevelopment along an urban waterfront at Victoria Dockside, Hong Kong

Hongning Lan[a], Kevin Ka-Lun Lau[a,b,c,*] , Yuan Shi[a,c], Chao Ren[a,d]

[a] Institute of Future Cities, The Chinese University of Hong Kong, Hong Kong

[b] CUHK Jockey Club Institute of Ageing, The Chinese University of Hong Kong, Hong Kong

[c] Institute of Environment, Energy and Sustainability, The Chinese University of Hong Kong, Hong Kong

[d] Faculty of Architecture, University of Hong Kong, Hong Kong

*Corresponding author:

Tel.: +852 3943 5398

E-mail address: kevinlau@cuhk.edu.hk (K.K-L. Lau)

Postal address: Institute of Future Cities, Room 406B, Wong Foo Yuan Building, The Chinese University of Hong Kong, Hong Kong

Highlights

- Design scenarios of a waterfront redevelopment was evaluated using the ENVI-met model.
- Different mitigation strategies lead to synergistic improvement to local microclimate.
- Building form and ventilation corridor enhance the surrounding wind environment.
- Green façades show higher cooling potential in street canyons in high-density context.
- Climate-sensitive design strategies effectively improve pedestrian thermal comfort.

Improved urban heat island mitigation using bioclimatic redevelopment along an urban waterfront at Victoria Dockside, Hong Kong

Abstract

Bioclimatic design provides solutions to mitigating the urban heat island (UHI) effect and improving urban quality of life. Waterfront settings provide a unique opportunity for UHI mitigation, as cool winds (i.e. sea breezes) provide good cooling conditions. We used ENVI-met numerical simulations to investigate the synergistic mitigation effects of redeveloped urban forms, ventilation corridors, and extensive greenery on local microclimate and outdoor thermal comfort at an urban waterfront in Victoria Harbour, Hong Kong. The thermal performance along the waterfront and within an inner urbanised area was evaluated in three scenarios: existing configuration (Case A), redeveloped building form (Case B), and Case B with a ventilation corridor and extensive greenery added. In the study area's subtropical climate, the additional strategies used led to a synergistic improvement in microclimate and thermal comfort in both settings. The appropriate use of combined urban forms and ventilation corridors along waterfronts can thus lead to a more acceptable pedestrian-level wind environment and enhance the ventilation potential within inner urbanised areas. The cooling intensity of greenery (turf and green facades) along such waterfronts can also be extended for further benefits. Overall, the synergistic mitigation effects of redeveloped urban forms, ventilation corridors, and extensive greenery in proximity to water bodies demonstrated here provide science-based guidance for the use of bioclimatic design along urban waterfronts in order to achieve improved microclimates and thermal comfort at neighbourhood scales.

Keywords: Bioclimatic design; Waterfront; Mitigation strategies; Microclimate; Outdoor thermal comfort

1. Introduction

1.1. Background

Global warming has negative impacts on human health, agriculture, the economy, and the environment (IPCC, 2018). Urbanisation can result in extensive land-cover changes, dense urban development, and anthropogenic heat release, with environmental consequences including exacerbated warming in cities (Arnfield, 2003; Kwok et al., 2019). The urban heat island (UHI) effect, which refers to higher temperatures in city centres than in surrounding rural or suburban areas, is a common and well-documented climatic phenomenon in global cities. It can have negative health impacts such as heat-related illness, heat stress, and discomfort (especially in summer), affecting the quality of life in urban areas.

Urban redevelopment causes dramatic changes in land cover and urban form, modulating urban microclimates. Recently, bioclimatic interventions have been used during this process to create more comfortable urban spaces. For example, the use of cool materials, urban greening, and water (Battista et al., 2016; Karakounos et al., 2018) and adjustments in building form (Ng et al., 2011) directly affect the insolation and wind conditions of urban spaces. Therefore, urban redevelopment can be an opportunity to improve the quality of life in urban environments (Chan and Yung, 2004).

Hong Kong, a high-density urban city with a subtropical climate and many high-rise buildings, suffers from a severe UHI effect (Siu and Hart, 2013). The number of very hot days (daily maximum air temperature > 33°C) and very hot nights (daily minimum air temperature > 28°C) has increased dramatically in the last twenty years (Hong Kong Observatory, 2020). In addition, due to a lack of comprehensive urban planning in the past, high-density development in Hong Kong aggravated UHI, contributing to a series of social and environmental problems such as crowded living environments, traffic congestion, and poor environmental quality (Poirot, 1995). As many UHI mitigation strategies have been suggested and applied to diminish heat accumulation and mitigate its negative effects in urban areas (Lensky et al., 2015), a comprehensive assessment of such strategies is both a challenge and an opportunity of great importance for urban quality of life.

The Hong Kong Buildings Department launched the Sustainable Building Design (SBD) Guidelines in 2011, which provide quantitative guidelines for three key building design elements: building separation, building setback, and site greenery coverage ratio. The aim is to improve air ventilation at the pedestrian level based on building redevelopment and enhancing the environmental quality of living spaces in Hong Kong, further mitigating UHI. These guidelines also encourage developers and architects to take a more responsive role with respect to buildings' bulk, height, ventilation, greenery, and energy efficiency.

1.2. UHI mitigation strategies

Various UHI mitigation strategies aimed at alleviating excessive thermal stress have been proposed by city planners, including changes to urban form, ventilation, blue space, and greenery (Ouyang et al., 2020). These strategies generally rely on modifying the surface energy balance over built landscapes.

1.2.1. Urban form

The connection between urban form and UHI is well-established (Johansson and Emmanuel, 2006; Lin et al., 2013; Lau et al., 2016), as this can create canyons trapping heat and atmospheric pollutants. Urban canyon geometry is normally quantified by aspect ratio, street orientation, and sky view factor (SVF). Oke (1981; 1982) first identified the influence of urban density and canyon form on heat intensity in the 1970s and determined a clear positive logarithmic relationship between aspect ratio and the year-round maximum canopy layer using observations and a relatively simple model. Giannopoulou et al. (2010) performed measurements in three streets with different geometries and found a decrease in the diurnal temperature range and cooling rate with an increased aspect ratio. Takebayashi and Moriyama (2012) compared both east-west and north-south oriented streets against surface temperature measurements in Tokyo and found that the shading effect of a tall building in north-south street canyons had less impact on solar gain than that for east-west streets. Tall buildings and narrow canyons reduce SVF and increase the amount of shaded area at the surface, resulting in lower temperatures in canyons during daytime but higher temperatures at night (Elnaha, 2003; Svensson, 2004; Unger, 2009). However, some studies have shown that SVF is positively related to air temperature, regardless of time (Yang et al., 2011; Wang et al., 2016; Lan and Zhan, 2017; Yin et al., 2018).

1.2.2. Urban ventilation

Urbanisation significantly modifies land-surface roughness as natural cover is replaced by built materials. Urban ventilation is also affected by urban form, as high buildings obstruct and separate winds, often resulting in low wind speeds at the pedestrian level. However, when several buildings are constructed in proximity, a higher wind speed can be squeezed through the narrow space (i.e., the Venturi effect). Less-ventilated urban areas exacerbate UHI intensity, leading to higher air temperatures and worse thermal comfort at the pedestrian level, especially in high-density built environments. Building porosity has drawn increasing attention in recent years as a way to improve the pedestrian-level ventilation potential in high-density cities. Yuan and Ng (2012) reported that implementing building porosity, including building setback, separation, and permeability, improved the pedestrian-level wind environment and thus outdoor thermal comfort in summer. Fan et al. (2017) compared isolated and non-isolated urban canyons and found that building porosity improved the pedestrian wind environment. Du et al. (2018) studied the porosity of an isolated building and a group of buildings, showing that a larger porosity generally resulted in better pedestrian wind comfort. An et al. (2018) also reported that building porosity enhanced ventilation in street canyons within urbanised areas, as in the use of open spaces included within structures themselves. However, such previous studies have mainly focused on the ventilation potential of building porosity in internal urban contexts, whereas comparable research on waterfronts is lacking despite the higher wind speeds occurring there (Tuller, 1995).

1.2.3. Urban blue space

Urban blue space is a nature-based element of urban land use and has long been considered a possible mitigation strategy for UHI. Its high thermal inertia and capacity, as well as low thermal conductivity and radiance, lead to lower surface temperatures and influence the ambient temperature of the surrounding

environment, especially during hot weather. Adams and Dove (1989) reported that a 35-metre-wide river caused an ambient temperature drop of 1–1.5 °C. Cheng et al. (2019) found that the cooling distance from a lake varied by land uses such as forest and farmland (462.5 m), impervious surfaces (400 m), lawn (326.5 m), and bare land (262.5 m). Hathway and Sharples (2012) reported that urban form on the banks of the UK's River Don, such as walls or buildings, quickly cut off the water's cooling potential. He et al. (2020) found that the ventilation performance of a compact high-rise gridiron precinct in coastal Sydney (influenced by sea breezes) significantly mitigated UHI and improved relative humidity, significantly improving outdoor thermal comfort. Nevertheless, interactions between building form, local ventilation, and UHI effects in waterfront settings in a subtropical climate have not been well studied.

1.2.4. Urban greenery

Urban greening is one of the most promising strategies for mitigating heat stress and improving thermal comfort because of the complementary mechanisms of shading and evapotranspiration. This can include street greenery, green roofs, and green facades. Carefully sited street greenery can block solar radiation and reduce heat stored on surfaces and facades (Klemm et al., 2015), and can convert solar radiation into latent heat through evapotranspiration, lowering both air and surface temperatures below tree canopy. Ng et al. (2012) showed that 33% of tree planting in urban areas lowered pedestrian-level air temperature by approximately 1 °C in Hong Kong. Lobaccaro and Acero (2015) showed that combining the presence of trees and grass a typical urban street canyon in Bilbao effectively improved the pedestrian-level thermal comfort with the highest physiological equivalent temperature (PET) reduction of 10 °C. Davtalab et al. (2020) found that green space had a more prominent effect on air temperature and mean radiant temperature than other meteorological parameters; at vegetated locations, mean air temperature was 1 °C lower, mean radiant temperature was 6 °C lower, and PET was 7 °C lower than non-vegetated locations.

Green roofs are a feasible design strategy for microclimate amelioration and energy conservation (Liu et al., 2012). For example, Wong et al. (2003) showed that a rooftop garden on a low-rise building in Singapore contributed thermal benefits to both the building and its surrounding environment. However, the mitigation potential of green roofs varies with building height. found that the mitigation potential at street level was almost negligible when green roofs were installed on high-or medium-rise buildings in Tokyo (Chen et al., 2009) and Hong Kong (Ng et al., 2012).

Although green facades have significant potential for surface temperature reduction (Wong et al., 2010; Sternberg et al., 2011), conflicting conclusions exist regarding the cooling potential of ambient air temperature at the neighbourhood scale. De Jesus et al. (2017) found in situ air temperature reductions of 2.5–2.9 °C when comparing green and bare walls in Madrid, Spain. Morakinyo et al. (2019) showed that 30–50% of facade surface area in high-density Hong Kong urban canyons must be greened to reduce daytime and night time air temperatures by approximately 1 °C. However, Hoelscher et al. (2016) showed no ambient cooling effect for three green facades in Berlin urban canyons during hot summer conditions.

Recently, an increasing number of researchers has focused on the synergistic cooling effects of greenery and blue space. Xu et al. (2010) showed that improved thermal comfort could be extended throughout a 10–20 m zone using littoral vegetation (grass and trees) along the waterfront of Shanghai's Huangpu River. Hathway et al. (2012) reported that high levels of vegetation next to a river increased cooling on the bank, with the most extensive cooling distribution about 30 m from the river's centre. Shi et al. (2020) focused

on the synergistic cooling effects of different land uses (forest, lawn, and impervious pavement) and lakes in Chongqing, showing that tree species with low leaf area index had a greater cooling effect on the surrounding water's thermal environment. However, few observational studies have explored the cooling potential of green facades and green roofs along waterfronts in inner urbanised areas, especially for high-density cities in a subtropical climate.

1.3. Study objectives

Although previous studies have focused on the UHI mitigation effects of urban form, ventilation, and greenery in isolation, they have not considered the mitigation effects of applying these synergistically along waterfronts and within inner cities. In addition, researchers have mainly focused on the penetration effect of building porosity in an urban context, while the combined effects of building porosity and urban form along waterfronts on local ventilation and UHI have not been well studied. Furthermore, the cooling effects of green facades and roofs along waterfronts in inner urbanised areas have not been fully investigated, especially in high-density cities in a subtropical climate. There is a clear need to better understand the role of bioclimatic design and UHI mitigation strategies in urban redevelopment along urban waterfronts. Therefore, we conducted a parametric study in high-density Hong Kong using ENVI-met software to (1) expand on existing knowledge of the synergistic effects of UHI mitigation strategies on the microclimates and outdoor thermal comfort of urban waterfronts and (2) contribute to a better understanding of bioclimatic design strategies for more appropriate urban redevelopment.

2. Methodology

2.1. Study area

Hong Kong is situated on the east side of the Pearl River estuary (22°15'N, 114°10'E) and is surrounded by the South China Sea on all sides except the north. The region has a sub-tropical climate, but the combination of vast surrounding water bodies and tropical latitude gives Hong Kong a warm and humid climate. The daily mean air temperature and relative humidity in summer are generally around 28.5 °C and 80%, respectively, with air temperatures often exceeding 31 °C in the afternoon (Cheung and Jim, 2018).

Hong Kong is famous for its high population density and high-density high-rise urban morphology. It is one of the most densely populated cities in the world at 6,244 people per km^2 in urban areas. According to the 2011 Population Census, its most populated districts were concentrated in the main urban areas, particularly in the Kowloon Peninsula. High population and limited land resources have resulted in high-density high-rise urban morphology in downtown areas, whose compact urban morphology results in intensive UHI and insufficient ventilation.

As water bodies have long been considered capable of mitigating UHI, we investigated the potential of bioclimatic design along the Hong Kong waterfront to achieve this, focusing on 640,000 m^2 within the Tsim Sha Tsui district as the numerical simulation area (Figure 1a). This redevelopment site is located next to Victoria Harbour and consists of two buildings with heights of 63.4 m and 50.0 m. The area is surrounded by intensive high-rise commercial and residential buildings to the north and public buildings to the west

(Figure 1b). To the east and west is Victoria Harbour, which can bring a continuous moist sea breeze to the inner Kowloon Peninsula. Although two parks (Signal Hill Garden and Salisbury Garden) surround the study area, greenery is still limited inside the parks.

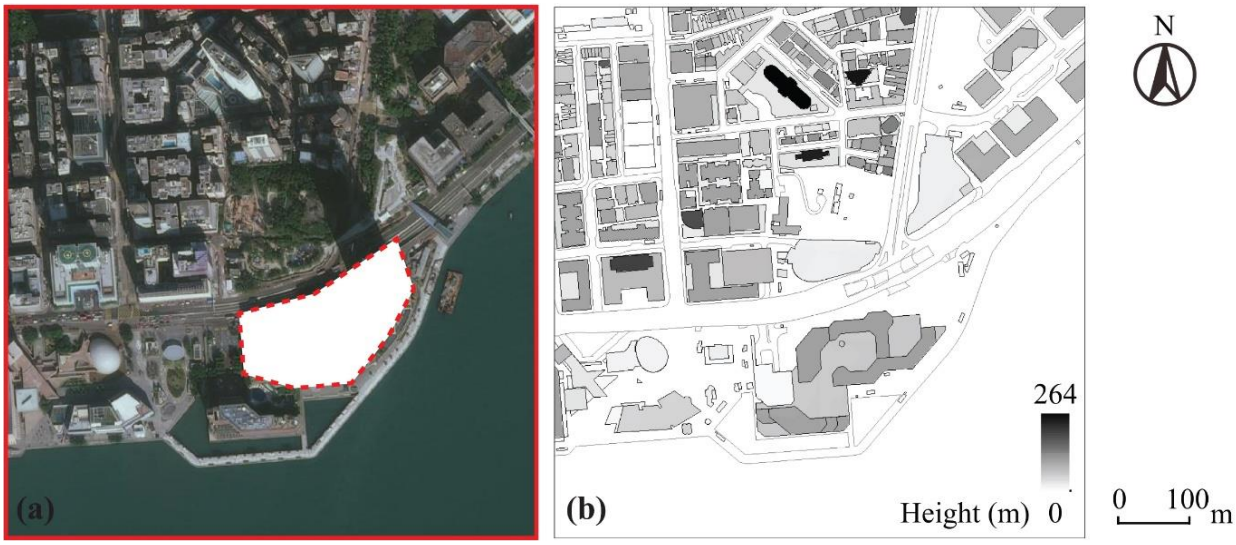

Figure 1. (a) Satellite image of the study area and (b) distribution of building height in the study area.

2.2. Microclimatic measurements

Microclimatic measurements were conducted from 10:00 on 25 September 2019 to 10:00 26 September 2019 at designated points (Figure 2). P1 was located on the sidewalk of the east-west oriented main street at the northern boundary of the study area, P2 was located inside the north-south oriented ventilation corridor, and P3 was located in a rooftop garden 40 m above the ground. The mobile meteorological station consisted of a TESTO 480 data logger for measuring air temperature (T_a), relative humidity (RH), wind speed (v), and a globe thermometer to measure the globe temperature (T_g). The globe thermometer consisted of a thermocouple wire (TESTO flexible Teflon type K) held inside a black painted table tennis ball with a diameter (D) of 38 mm and emissivity (ε) of 0.95. The mean radiant temperature (T_{mrt}) was determined using the following equation from Thorsson et al. (2007):

$$T_{mrt} = \left[\left(T_g + 273.15\right)^4 + \frac{1.10*10^8*v^{0.6}}{\varepsilon*D^{0.4}}\left(T_g - T_a\right)\right]^{1/4} - 273.15 \quad (1)$$

2.3. ENVI-met simulation

2.3.1. Model description

ENVI-met is a holistic three-dimensional non-hydrostatic microclimate model intended for the simulation of surface-plant-air interactions in a complex urban environment based on computational fluid dynamics and thermodynamics, with a typical resolution of 0.5–5 m in space and 1–5 s in time (Bruse and Fleer,

1998). This model has been applied to urban microclimate environments by many researchers in different regions and has been shown to accurately calculate the diurnal profile of microclimate variables (Kong et al., 2016; Tan et al., 2016). We used ENVI-met V4.4.4 Winter19/20, into which new full-forcing and green-facade modules have been integrated, to simulate thermal comfort. The full-forcing module allows users to set diurnal cycles of boundary conditions that are not limited to 24 h of data and to input more user-defined meteorological parameters such as radiation and cloud cover. Additional profiles for air temperature, air humidity, wind speed, and wind direction can be entered for different heights depending on their measurement height. The green-facade module can simulate the effects of wall and roof greening on building energy performance and outdoor microclimate. Both modules were used in this study.

Figure 2. Location of the measurement points in the study area.

2.3.2. Model setup

All simulations were set to represent Hong Kong's subtropical hot-humid summer climate, using hourly air temperature, relative humidity, and prevailing daytime and nighttime wind speed data from June to August 2009–2018 (averaged as 24 hr data), obtained from the two nearest weather stations (Hong Kong Observatory and Star Ferry, Figure 3). As observations in Hong Kong only measure global solar radiation, we obtained direct shortwave solar radiation, diffuse short radiation, and downwelling longwave radiation from site measurement data. Because the intervals for ENVI-met input meteorological data must be 30 min in full forcing module, hourly meteorological data were interpolated into 30 min data, and linear interpolation was used for air temperature, relative humidity, wind speed, shortwave radiation, and longwave radiation. Figure 4 shows 30 min meteorological data for a typical summer day.

The simulation domain was filled by 200×200 horizontal grids at 4 m resolution and 50 vertical grids with 4 m resolution and 15% telescoping from a height of 120 m. Considering the numerical simulation stability and accuracy, the model area was rotated 4° clockwise from north to reduce the geometric complexity. Twenty empty physical grids were left between the model core area and each side of the boundary to decrease the blockage ratio of buildings to the total cross-sectional area of the domain along the inlet wind direction. All buildings were assumed to be made of concrete with a wall and roof albedo of 0.3; the

road albedo was set to 0.2. The soil humidity of different layers was set to default, and the initial temperature of different layers was obtained from the Hong Kong Observatory. Trees, grass, and green facades and roofs were set to default (0100T1, 000000, and 01AGDS, respectively). The simulations started at 00:00 and ran for a continuous period of 48 hr, while the data analysis was focused from 07:00 on the first day to 06:00 on the second day to capture daytime and nighttime periods (the previous data were taken as spin-up phases). All input parameters are given in Table 1.

Figure 3. Satellite view of Hong Kong Observatory (HKO) and Star Ferry (SF) from ArcGIS.

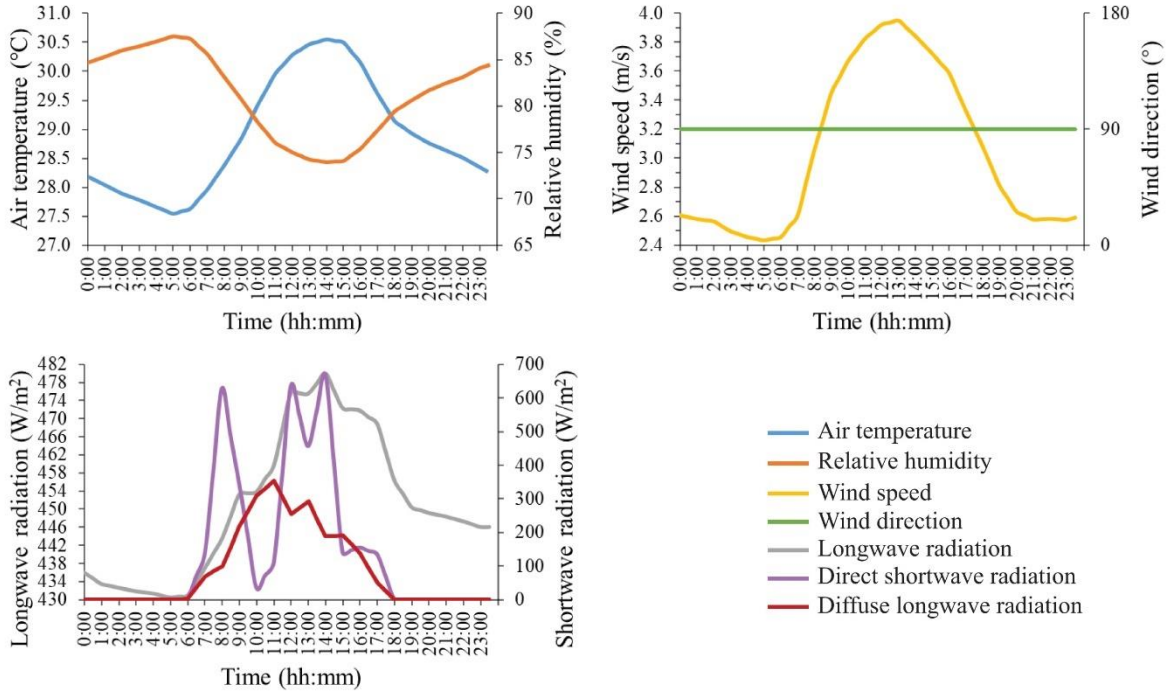

Figure 4. 30-minute temporal resolution meteorological data of the typical summer day.

2.3.3. Simulation scenarios

The numerical simulations were made up of three scenarios with a domain area of 800 × 800 m, including the previous building configuration (Case A), a redeveloped building configuration (Case B), and Case B with the adoption of a ventilation corridor and extensive greenery (Case C) (Figure 5). The differences between the three scenarios were mainly focused on the building form, ventilation corridor, and greenery. Case A consisted of four high-rise buildings with an average height of 56 m and a floor area of approximately 33,500 m^2. Greenery (grass and trees) were mainly located in the western part of the site, next to Salisbury Garden. In Case B, the two existing buildings were replaced by one podium block and two high-rise buildings with heights of 34 m, 100 m, and 274 m. In Case C, in addition to the redeveloped buildings consisting of one podium and two high-rise buildings with the average heights of 45 m, 100 m, and 280 m, several additional mitigation strategies based on SBD guidelines were applied:

- Ventilation corridor: Two ventilation corridors (Figure 6) were integrated in the buildings. One was 20 m wide and 8.4 m high, at ground level in alignment with Chatham Road, and the other was 12.5 m wide and 27 m high, above the podium block.
- Extensive greenery: Green facades were provided along the west-oriented and north-oriented facades with a total area of 3770 m^2. Street greenery was planted along Salisbury Road, and further greenery was installed on the flat podium roof, with a total area of 9661 m^2. Overall, more than 34% of the site area was covered with greenery (Figure 6).

Table 1. Summary of input parameters and values for numerical simulations

Parameter	Definition	Input Values
Meteorological conditions	Air temperature[1] (%)	Hourly profile in Figure 4
	Relative humidity[1] (%)	
	Wind speed[2] (m/s)	
	Wind direction[2] (°)	100
	Soil humidity (%)	Default
	Soil initial temperature[1] (°C)	Upper layer (0-20 cm): 30.35 Middle layer (20-50 cm): 30.33 Deep layer (50-200 cm): 29.05 Bedrock layer (below 200 cm): 27.40
	Cloud cover (Oktas)	1
Building information	Wall and roof albedo	0.3
Road information	Road albedo	0.2
Tree information	Tree height (m)	10
	Vertical LAD profile	0.00,0.00,2.18,2.18,2.18,2.18,2.18,2.18,1.72,0.00
Grass information	Grass height (m)	0.63
Green façade and roof information	Plant height (m)	0.3
	Leaf area index (LAI)	1.5m^2/m^2

[1] Obtained from Hong Kong Observatory (HKO)
[2] Obtained from Star Ferry (SF)

2.4. Data analysis

The simulation's meteorological outputs (air temperature, mean radiant temperature, relative humidity, and wind speed) were imported into Biomet to calculate PET at the pedestrian level (2 m). In addition, we selected two points P1 (Avenue of Stars) and P2 (waterfront open space) where major activities occur and seven roads within urbanised areas (R1, Salisbury Road; R2, Chatham Road S; R3, Minden Ave; R4, Mody Road; R5, Nathan Road; R6, Peking Road; R7, Middle Road) as analysis points and areas to evaluate microclimate changes and improvements in outdoor thermal comfort (Figure 7). Averaged data within the analysed areas for each road were reported as a single value to represent their microclimate and thermal conditions. The individual and synergistic cooling effects of the mitigation strategies were then quantified based on the differences in air temperature (T_a), mean radiant temperature (T_{mrt}), wind speed (v), and PET. The cooling effect of the standalone redeveloped building form was calculated as the difference between Cases B and A, the cooling effects of the ventilation corridor and extensive greenery were calculated as the difference between Cases C and B, and the synergistic cooling effects were calculated as the difference between Cases C and A.

To assess the effects of extensive greenery, apart from the above-mentioned P2 used to quantify the cooling potential of turf, two further points were selected in case C for analysis: one tree on the sidewalk beside the redeveloped building (T1) and one exposed area (E1), as well as ten points on the green facade (GF1, GF2, GF3, and GF4), bare facade (BF1 and BF2), green roof (GR1 and GR2), and bare roof (BR1 and BR2) (Figure 8). The values from the grids next to each tree were averaged as a single value to represent the conditions for each tree. For test points from the facade and roof, averaged values from points with the same orientation and surface type (categorised as north-oriented green facade (GF(N)) and bare facade (BF(N)), west-oriented green facade (GF(W)), and bare facade (BF(W)), as well as green rooftop (GR) and bare rooftop (BR)) were reported as a single value to represent the conditions of green and bare surfaces with the same orientation. As many previous studies have characterised the cooling effects of trees, green facades, and green roofs by calculating the differences between areas with and without greenery (Morakinyo et al., 2017), differences in T_a ($\Delta T_a = T_{a(tree)} - T_{a(exposed)}$) between areas with and without trees and differences in surface temperature ($\Delta T_s = T_{s(green\ surface)} - T_{s(bare\ surface)}$) between green and bare surfaces were calculated to quantify the cooling effects on microclimate and thermal comfort.

Figure 5. Visualization of the ENVI-met models of Cases A, B and C.

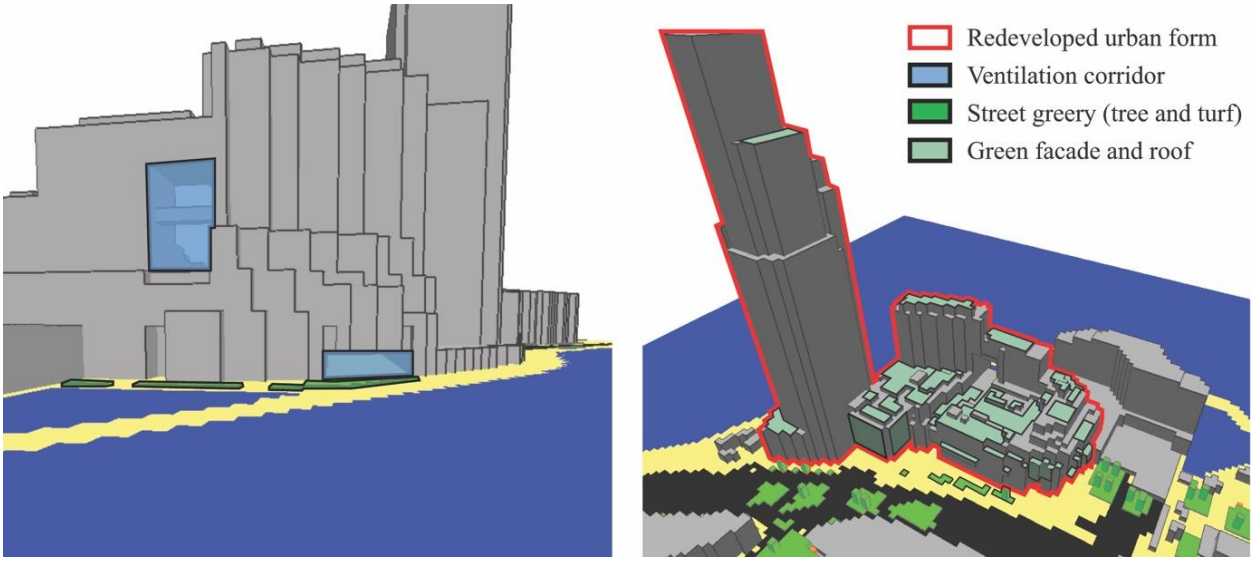

Figure 6. Mitigation strategies based on SBD Guidelines in Case C.

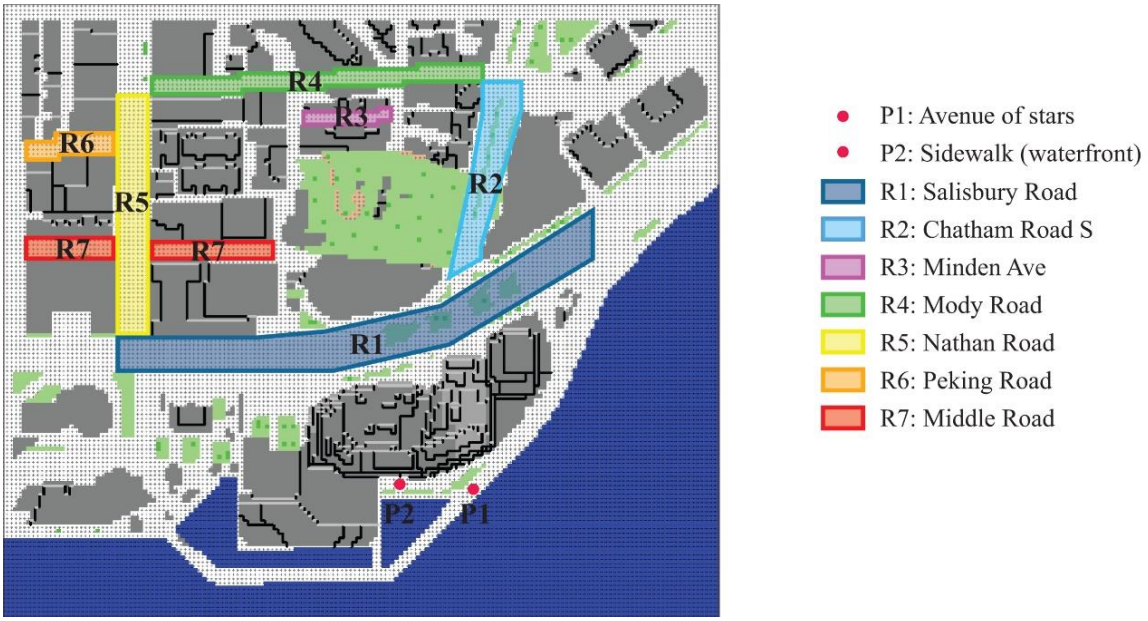

Figure 7. Schematic diagram of the locations of selected test points and areas.

3. Results

3.1. Evaluation of the ENVI-met model

Field measurements were taken to obtain microclimatic information in order to evaluate the performance of the ENVI-met model (Figure 9). The measured and simulated T_a had strong correlation, with R^2 for P1,

P2, and P3 of 0.98, 0.95, and 0.94, respectively. The measured and simulated T_{mrt} had reasonable correlation, with R^2 for P1, P2, and P3 of 0.88, 0.79, and 0.87, respectively. However, the wind speed simulation was less satisfactory, with the highest R^2 being only 0.54 at P1. The wind speed in the ventilation corridor was even less satisfactorily simulated (R^2 of 0.35), probably due to the location of the measurement point at the entrance of the main road, where the air flow was heavily affected by road traffic. Overall, the ENVI-met model performed well in simulating the microclimatic environment of the study area and its immediate surroundings.

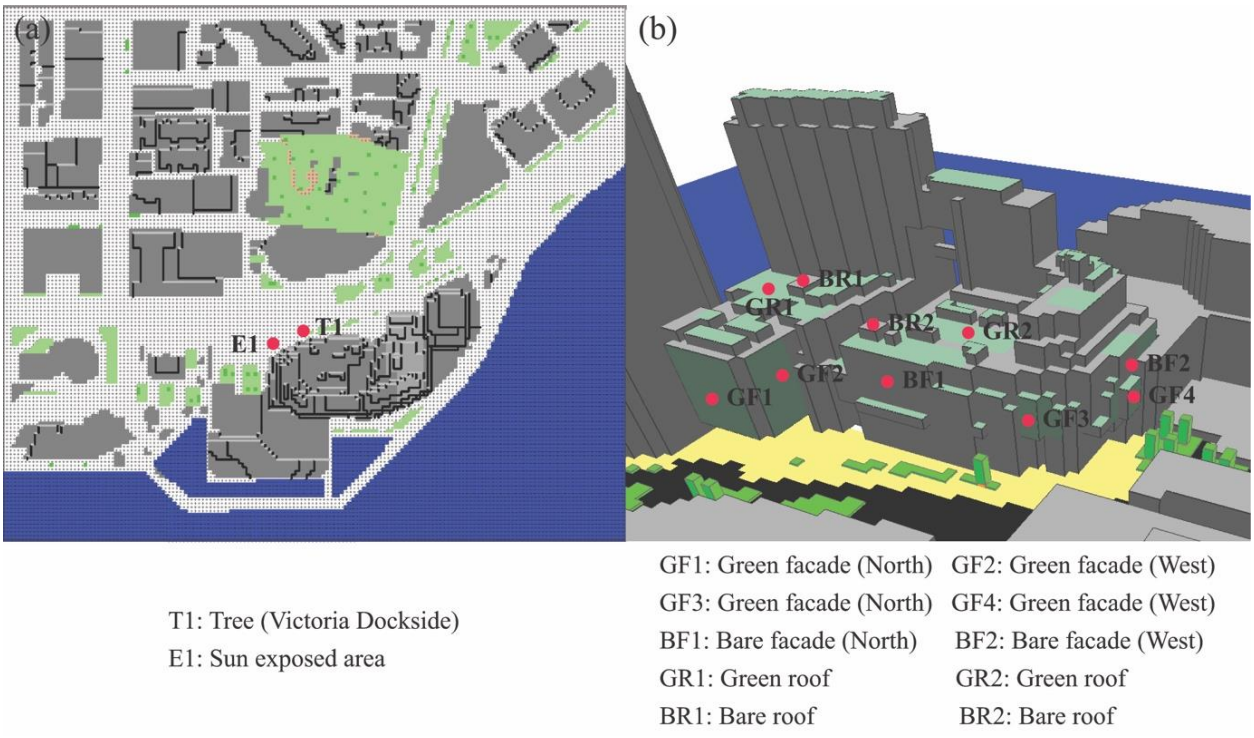

Figure 8. (a) Schematic diagram of selected trees and exposed area in Case C (b) Schematic diagram of selected test points at green façade (GF1, GF2, GF3 and GF4), bare façade (BF1 and BF2), green roof (GR1 and GR2) and bare roof (BR1 and BR2) in Case C.

3.2. Synergistic effects of waterfront UHI mitigation strategies

3.2.1. T_a between Cases A, B, and C

The mean T_a at P1 showed no obvious differences between Cases A, B, and C (Table 2). However, T_a at P2 in Cases B and C showed a mean decrease of 0.1 °C during daytime when compared with Cases A and B, respectively. There were a wide range of reasons contributing to this decrease. In Case B, a higher high-rise building provided more shading opportunities than in Case A, resulting in a lower T_a at P2. However, in Case C, the green roof and street greenery along the sidewalk may have led to a decrease in T_a. To further identify the cooling potential of the green roof and turf, we took the hottest time (15:00) as an example and compared the distribution of ΔT_a at pedestrian level (2 m) and at vertical levels of 14 m, 38

m, and 42 m between Cases C and B. The T_a decrease around P2 mainly occurred downwind of the turf (Figure 10), while the green roof contributed little to the decrease (Figure 11), suggesting that the turf was the primary cause of the decrease in T_a at P2. Overall, both the redeveloped building form and turf led to a synergistic mean T_a reduction of 0.2 °C at P2 between Cases C and A, with the highest reduction of 0.5 °C from 12:00 to 14:00.

Table 2. Differences between Cases B and A, Cases C and B as well as Cases C and A of hourly averaged T_a, V_a, T_{mrt} and PET within redeveloped area and inner urbanized area.

	Case B – Case A				Case C – Case B				Case C – Case A			
	ΔT_a (°C)	ΔV_a (m/s)	ΔT_{mrt} (°C)	ΔPET (°C)	ΔT_a (°C)	ΔV_a (m/s)	ΔT_{mrt} (°C)	ΔPET (°C)	ΔT_a (°C)	ΔV_a (m/s)	ΔT_{mrt} (°C)	ΔPET (°C)
P1: Avenue of stars												
Max.	±0.1	+0.2	-0.6	-0.6	±0.1	-0.2	±0.1	±0.2	-0.1	+0.1	-0.7	-0.4
Mean	0.0	+0.1	-0.3	-0.3	0.0	-0.1	0.0	+0.1	0.0	0.0	-0.3	-0.1
Min.	0.0	+0.1	-0.1	-0.1	0.0	0.0	0.0	0.0	0.0	0.0	0.0	0.0
P2: Sidewalk (waterfront)												
Max.	-0.4	-0.3	-0.8	+0.6	-0.2	-0.4	-0.3	+0.6	-0.5	-0.7	-1.0	+1.0
Mean	-0.1	-0.3	-0.3	+0.1	-0.1	-0.3	0.0	+0.4	-0.2	-0.6	-0.4	+0.5
Min.	0.0	-0.2	-0.1	-0.4	0.0	-0.1	0.0	+0.1	0.0	-0.3	-0.1	-0.2
R1: Salisbury Road												
Max.	-0.7	-0.1	-23.7	-10.3	-0.1	+0.1	+1.5	-0.2	-0.7	-0.1	-23.1	-10.3
Mean	-0.2	-0.1	-2.1	-1.0	-0.1	+0.1	+0.2	-0.1	-0.2	0.0	-1.9	-1.0
Min.	-0.1	-0.1	-0.1	0.0	0.0	+0.1	0.0	0.0	0.0	0.0	-0.1	0.0
R2: Chatham Road S												
Max.	-0.2	+0.1	-0.8	-1.3	-0.1	+0.1	±0.1	-0.5	-0.2	+0.2	-0.8	-1.8
Mean	-0.1	+0.1	-0.3	-0.5	0.0	+0.1	0.0	-0.2	-0.1	+0.2	-0.3	-0.7
Min.	0.0	+0.1	-0.1	-0.2	0.0	0.0	0.0	-0.1	0.0	+0.1	-0.1	-0.3
R3: Minden Ave												
Max.	0.0	0.0	-0.5	-0.2	+0.1	+0.5	±0.1	-1.1	±0.1	+0.5	-0.6	-1.2
Mean	0.0	0.0	-0.2	0.0	0.0	+0.3	0.0	-0.4	0.0	+0.2	-0.2	-0.5
Min.	0.0	0.0	0.0	0.0	0.0	+0.2	0.0	-0.3	0.0	+0.1	0.0	-0.3
R4: Mody Road												
Max.	0.0	0.0	-0.5	-0.2	+0.1	+0.4	±0.1	-1.5	0.0	+0.4	-0.5	-1.6
Mean	0.0	0.0	-0.2	0.0	0.0	+0.3	0.0	-0.5	0.0	+0.2	-0.2	-0.5
Min.	0.0	0.0	0.0	0.0	0.0	+0.2	0.0	-0.3	0.0	+0.2	0.0	-0.3
R5: Nathan Road												
Max.	-0.1	0.0	-0.5	-0.2	+0.1	+0.2	±0.1	-1.1	-0.1	+0.2	-0.6	-1.2
Mean	0.0	0.0	-0.2	0.0	0.0	+0.1	0.0	-0.4	0.0	+0.1	-0.2	-0.4
Min.	0.0	0.0	0.0	0.0	0.0	+0.1	0.0	-0.2	0.0	0.0	0.0	-0.1
R6: Peking Road												
Max.	-0.1	-0.1	-0.5	-0.3	0.0	+0.9	±0.1	-1.6	0.0	+0.9	-0.5	-1.5
Mean	0.0	0.0	-0.2	0.0	0.0	+0.4	0.0	-0.7	0.0	+0.4	-0.2	-0.8
Min.	0.0	0.0	0.0	0.0	0.0	0.0	0.0	0.0	0.0	0.0	0.0	0.0
R7: Middle Road												
Max.	-0.2	-0.2	-0.5	+0.4	-0.1	+0.3	±0.1	-1.0	-0.2	+0.2	-0.6	-0.6
Mean	-0.1	-0.2	-0.2	+0.1	0.0	+0.2	0.0	-0.3	-0.1	0.0	-0.2	-0.2
Min.	0.0	-0.2	0.0	0.0	0.0	+0.2	0.0	-0.2	0.0	0.0	0.0	0.0

As for the roads within inner urbanised areas, the mean T_a at R1, R2, and R7 in Case B was slightly lower than in Case A, with a mean decrease of 0.2 °C, 0.1 °C, and 0.1 °C, respectively. At 15:00, the distribution of ΔT_a between Cases B and A mainly occurred in the western and middle part of R1, southern part of R2,

and eastern part of R7, ranging from 0.1 °C to 0.6 °C (Figure 11). Moreover, the T_a at pedestrian level along the R1 sidewalk within the redeveloped area was reduced by up to 0.2 °C between Cases B and A. Although shading opportunities provided by redeveloped high-rise buildings have the potential to reduce T_a, R1 was not included in the shaded area at 15:00 as shade mainly occurred in the eastern part of the redeveloped area. We further compared the distribution of ground T_s at 15:00 (Figure 12) between Cases B and A and found that the newly constructed building in the north-eastern part of the redeveloped area in Case B (an exposed area in Case A) may have contributed to the T_a reduction. The exposed area in Case A received more solar radiation than the redeveloped building area in Case B, resulting in higher ground T_s at the intersection of R1 and R2. When the cooling sea breeze from the east penetrated the intersection, higher ground T_s in Case A may have transferred more heat energy to the air than in Case B, resulting in a higher T_a at R1.

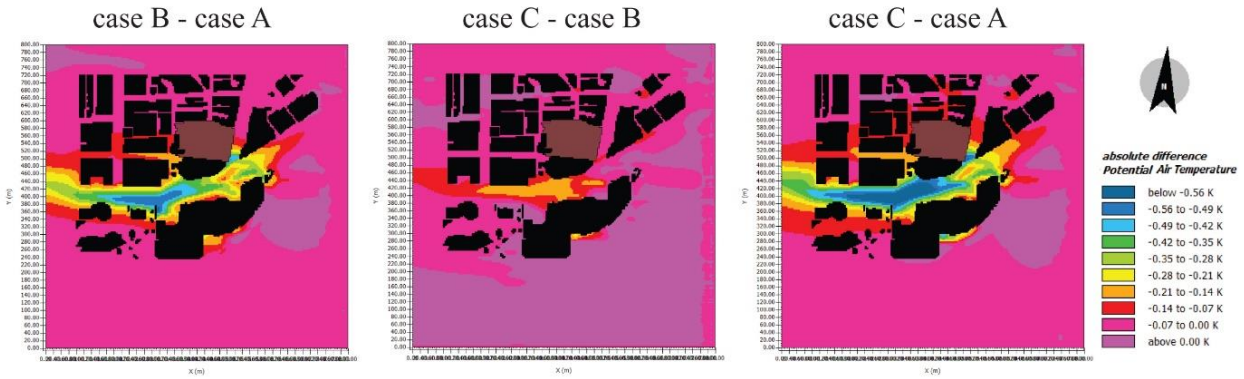

Figure 10. Distribution of ΔT_a at 15:00 between Cases B and A, Cases C and B as well as Cases C and A at pedestrian level.

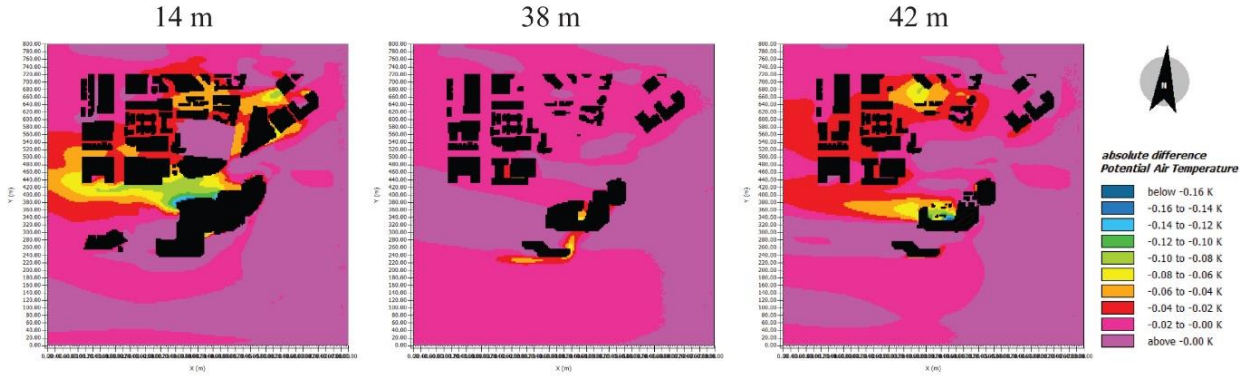

Figure 11. Distribution of ΔT_a at 15:00 between Cases C and B at vertical levels of 14m, 38m and 42m.

Comparing Case C with Case B, the mean T_a at R1 showed a reduction of about 0.1 °C from 14:00 to 17:00, with the highest reduction occurring at 15:00 (Figure 10). In addition, the cooling area in Case C was expanded 50 m further north than in Case B at 15:00. The existence of a green facade may be responsible for the mean T_a reduction and cooling area expansion, as T_a in front of the green facade at 14 m height contributed to a mean decrease of approximately 0.1 °C (Figure 11). Although the green roof showed the cooling potential of T_a on the podium rooftop, a negligible cooling effect was observed at 38 m height. However, no obvious difference in mean T_a at night was observed between Cases C and B. Overall, the

redeveloped building form and green facade in Case C exhibited daytime cooling potential mainly at R1, R2, and R7 compared with Case A, with a synergistic mean T_a reduction of 0.2, 0.1, and 0.1 °C, respectively.

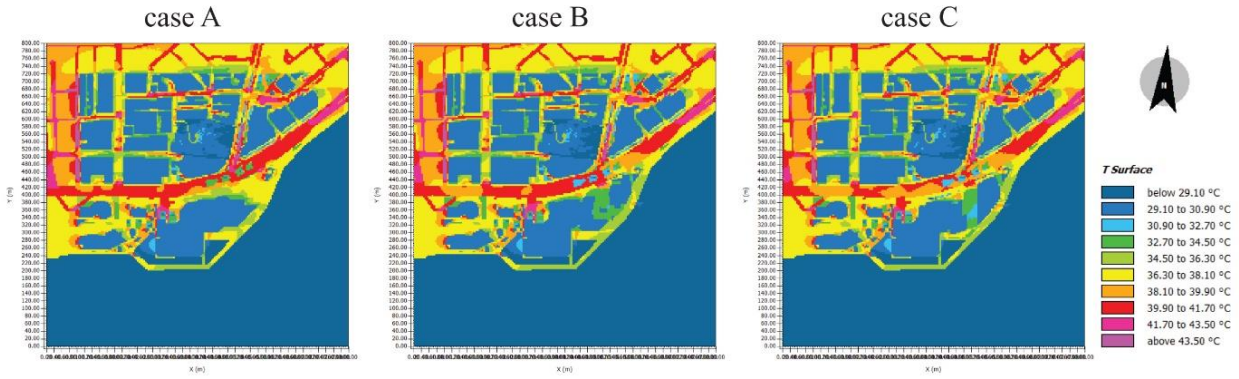

Figure 12. Distribution of T_s at ground level at 15:00 in Cases A, B and C.

3.2.2. Comparison of wind speed between Cases A, B, and C

Comparing Cases C and B, the pedestrian-level wind environment at all roads improved, with a mean V_a increase of nearly 0.2 m/s (Figure 13). The ventilation corridor was the predominant reason for this, as the V_a at test points inside the ventilation corridor at the pedestrian level and podium level (2 m above the podium roof) reached up to 1.1 and 1.2 m/s (Figure 14), resulting in higher wind permeability and ventilation potential in the inner urbanised area. Furthermore, E-W roads showed higher V_a increases than N-S roads, likely due to the prevailing easterly winds.

Apart from R1, the redeveloped building form in Case B had little effect on pedestrian-level ventilation and even caused a mean wind speed decrease at R7 of 0.2 m/s. Although the mean V_a at R1 in Case C remained the same as Case A (1.7 m/s) and was slightly higher than Case B (1.6 m/s), the distribution of V_a at R1 showed significant differences. The intersection of R1 and R2 showed a relatively higher V_a in Cases B and C than in Case A, which could be described as the corner effect of the redeveloped high-rise building. In addition, the new high-rise buildings caused a lower V_a on the leeward side (wind shadow), especially at the sidewalk where daily activities occurred on the north side of the redeveloped area (Figure 15). For example, at 15:00, V_a at the north-side sidewalk mainly ranged from 1.2–2.0 m/s in Cases B and C, which was beneficial for providing thermal relief and a comfortable outdoor urban environment, based on a V_a of 1.5 m/s from the Air Ventilation Assessment (AVA) Guidelines (Planning Department, 2005). However, in Case A at 15:00, V_a at the sidewalk reached 2.8 m/s with a mean of 2.4 m/s. From the perspective of thermal comfort, this high V_a might not be acceptable, as Cheng and Ng proposed that a V_a of 1–2 m/s in the shade under Hong Kong's climate is required in summer (Cheng and Ng, 2006). Overall, the introduction of a ventilation corridor offsets parts of the streets' V_a decrease caused by the building blockage effect, making the street wind environment consistent or improved.

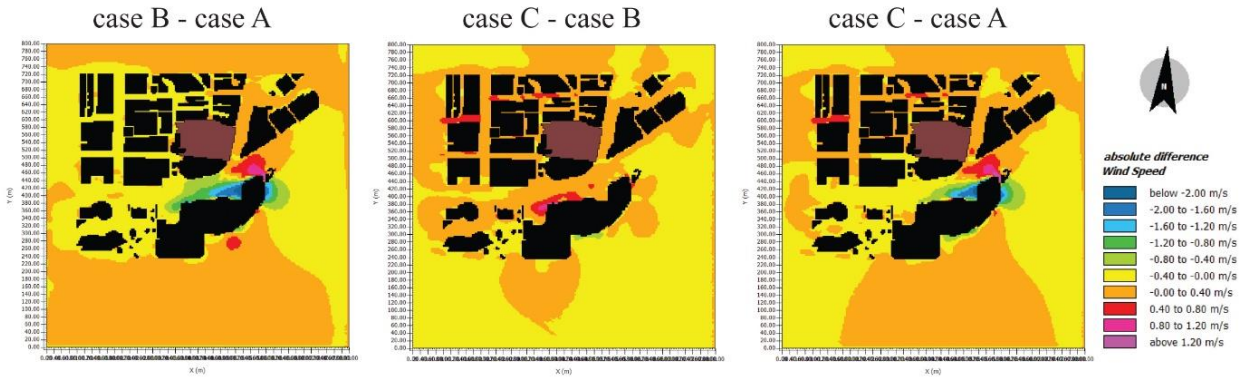

Figure 13. Distribution of ΔV_a at 15:00 between case B and A, case C and B as well as case C and A at pedestrian level.

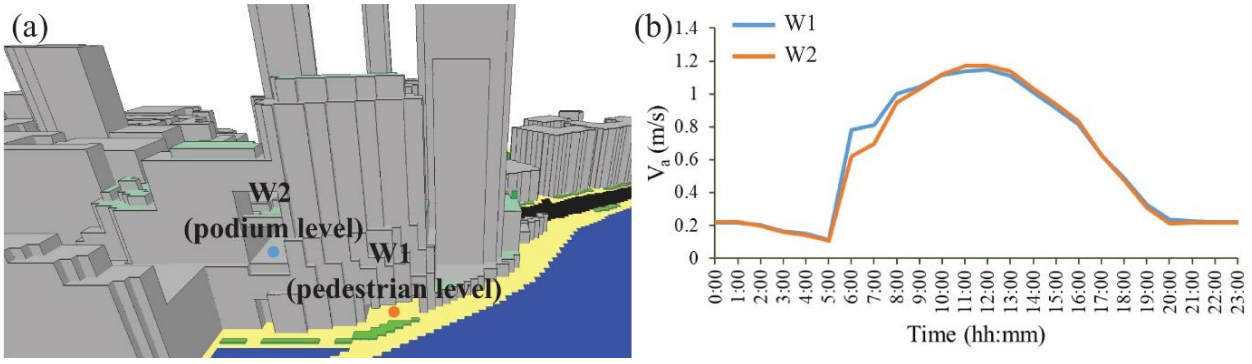

Figure 14. (a) Schematic diagram of test points inside the ventilation corridor at pedestrian level and podium level in Case C (b) Temporal variation of V_a inside the ventilation corridor at pedestrian and rooftop level in Case C.

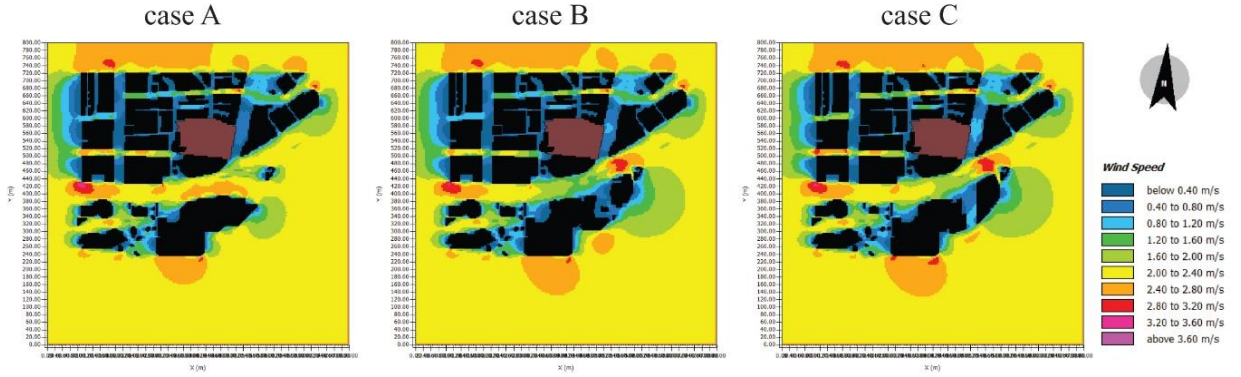

Figure 15. Distribution of V_a at 15:00 in Cases A, B and C at pedestrian level.

3.2.3. Comparison of T_{mrt} between Cases A, B, and C

Notable differences in T_{mrt} between Cases B and A as well as Cases C and A were found at the intersection of R1 and R2 and in the shaded areas provided by the redeveloped high-rise buildings. However, no obvious differences were observed between Cases C and A. For example, at 15:00 the mean T_{mrt} in the shaded areas in Cases B and C (eastern part of the redeveloped area) was reduced by up to 7 °C (Figure 16), mainly by the shading opportunity provided by the 274 m and 280 m high-rise buildings in Cases B and C, respectively. Moreover, the mean T_{mrt} in Cases B and C decreased by around 2 °C at the intersection of R1 and R2 (Figure 16), where a lower SVF (Figure 17) was observed due to the newly redeveloped buildings. The effect of redeveloped building form on radiation fluxes (especially longwave radiation flux) may contribute to this, resulting in T_{mrt} reduction (Lai et al., 2017).

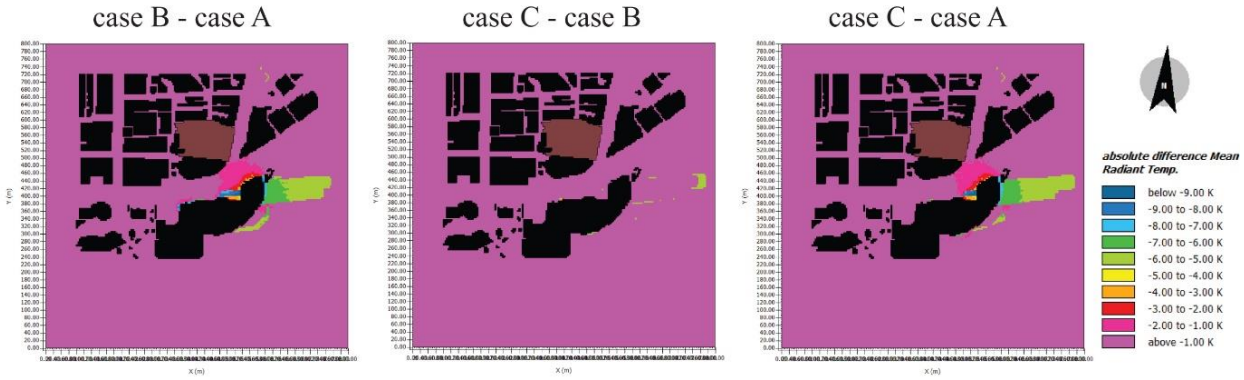

Figure 16. Distribution of ΔT_{mrt} at 15:00 between Cases B and A, Cases C and B as well as Cases C and A at pedestrian level.

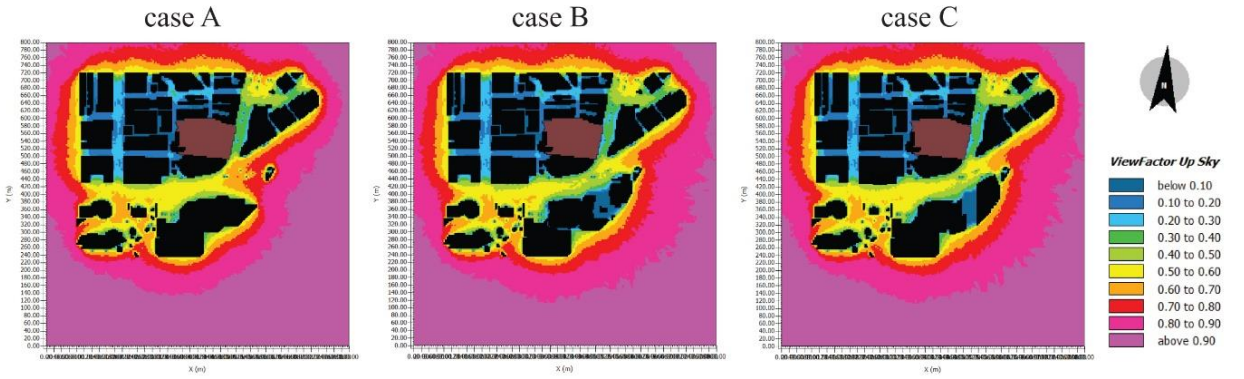

Figure 17. Distribution of SVF in Case A, case B and case C.

3.2.4. Comparison of PET between Cases A, B and C

Comparing Case B with Case A, mean PET showed a relative decrease at R1 and R2, with a mean reduction of 1.0 °C and 0.5 °C, respectively. At 15:00, notable ΔPET occurred mainly at the intersection of R1 and R2 (Figure 18), which may be affected by changes in T_a, V_a, and T_{mrt} caused by the newly redeveloped building.

Comparing Case C with Case B, the mean PET slightly decreased for all roads, ranging from 0.1–0.7 °C. This was mainly influenced by the higher pedestrian-level wind speed provided by the ventilation corridor. In addition, the green facade contributed to a lower T_a at R1, further improving the PET. Overall, the synergistic effects of the redeveloped building form, ventilation corridor, and green facade contributed to an overall decrease in mean PET for all roads of 0.2–1.0 °C.

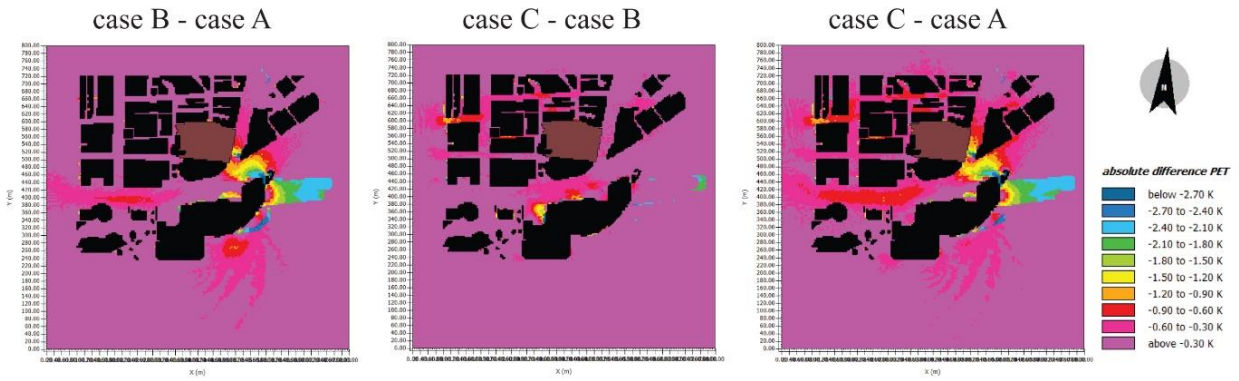

Figure 18. Distribution of ΔPET at 15:00 between case B and A, case C and B as well as case C and A at pedestrian level.

3.3. Cooling effect of extensive greenery

3.3.1. Cooling effect of trees on T_a

Figure 19 presents the hourly differences in T_a between areas with and without trees in Case C. Trees showed little cooling effect on pedestrian level T_a, as the highest reduction was only 0.1 °C. Although a previous study found that a 1 °C decrease in pedestrian-level T_a could be achieved by 33% tree coverage in Hong Kong (Ng et al., 2012), the rate of tree planting in our study was lower, contributing to ineffective street cooling. Moreover, because the trees were planted on the northern side of the project sites, they were mostly in shade, such that the difference in air temperature between locations under trees and the surrounding area was minimal; this implied that the selection of tree-planting location is important to the local microclimate (Tan et al., 2016). This further indicated that the green facade played a dominant role in the pedestrian-level T_a decrease at R1, compared with trees.

3.3.2. Cooling effect of green facade and green roof on T_s

Temporal variations in averaged T_s for the north-oriented facade, west-oriented facade, and rooftop, and the reduction in averaged T_s for these compared with bare surfaces, are presented in Figure 20. Overall, the mean surface temperature of greenery for the north and west facades was reduced by 2.0–7.5 °C (average 4.2 °C) and 1.1–13.8 °C (average 5.8 °C), respectively, compared to bare exterior walls with the same orientation. For the rooftop, the mean surface temperature showed the highest reduction (up to 23.9 °C, average 9.2 °C), as rooftops are more sunlit in the daytime than facades. Moreover, because of the increasing solar intensity, a higher reduction in surface temperature was observed during the daytime

with a diurnal average of 6.9 °C for the north-oriented facade, 9.1 °C for the west-oriented facade, and 16.1 °C for the rooftop. At nighttime, the surface temperature difference was not significant, with a nocturnal average of 2.5 °C for both facades and 2.4 °C for the rooftop. These results demonstrated that green facades and roofs were effective at exterior surface temperature reduction.

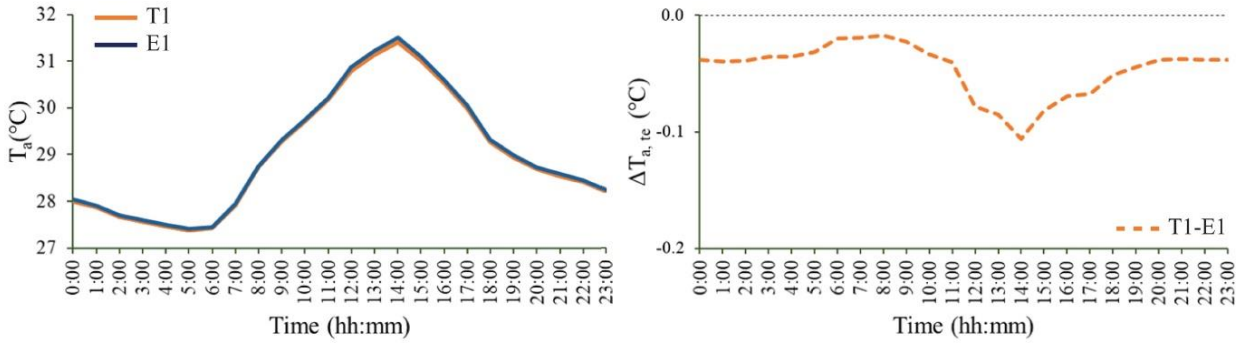

Figure 19. Temporal variation of T_a for test points and hourly differences of T_a between areas with and without trees in Case C.

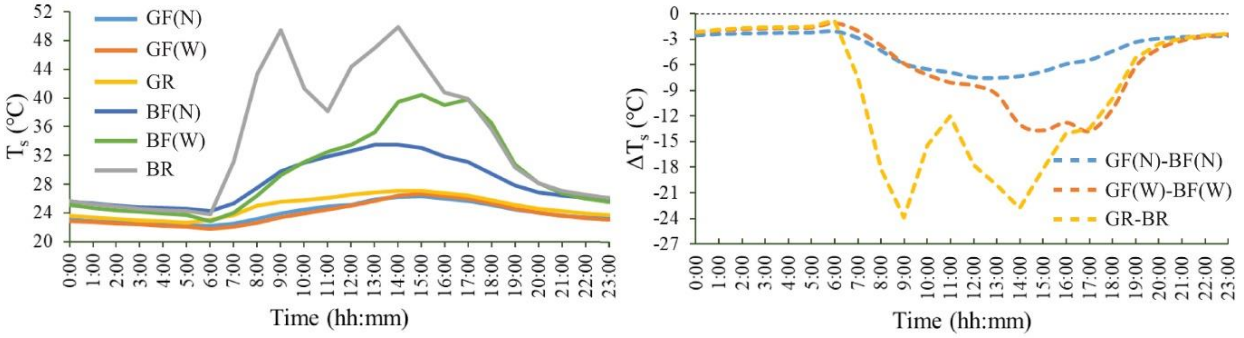

Figure 20. Temporal variation of T_s of North-oriented façade, West-oriented façade and rooftop and the reduction of T_s of façade and rooftop comparing with bare surfaces in Case C.

4. Discussion

4.1. Effect of UHI mitigation strategies on microclimate change and thermal comfort improvement

Although the synergistic effect of mitigation strategies does not sum in a linear fashion, microclimates and thermal comfort along waterfronts and within urbanised areas benefit from improved building forms, ventilation corridors, and extensive greenery. The redeveloped of higher buildings creates expanded shading opportunities, resulting in lower T_a and T_{mrt} in shaded areas during daytime. PET values decreased by 0.5–1.0 °C, corresponding to approximately a one-class change in the Hong Kong Urban Climatic Map (Planning Department, 2016). Therefore, adopting mitigation strategies at redevelopment sites can improve outdoor thermal comfort in surrounding locations without any significant modifications to urban geometry at the local level. In addition, as the north-eastern part of the redeveloped high-rise building was located further north in Cases B and C than in Case A, the building blocked the eastern sea breeze and resulted in lower V_a on the leeward side (wind shadow), especially along sidewalks where daily

activities occurred. This provided improved thermal relief and a more comfortable outdoor urban environment, as V_a remained ~1.5 m/s at R1 in Cases B and C compared with ~2.0 m/s in Case A. This indicated that the proper layout of high-rise buildings along a waterfront can block sea breezes and create a better pedestrian-level wind environment in leeward areas, despite the fact that this slightly decreases wind speed within inner urbanised areas. However, the ventilation corridor was capable of conducting wind into the inner urbanised area, offsetting some of the street V_a decrease caused by the building blockage effect. Therefore, redeveloped building forms and ventilation corridor proximity to the waterfront should be considered together to improve the wind environment along waterfronts and within inner urbanised areas. Any localised wind environment along a waterfront should be handled carefully according to its environmental setting (Ng, 2009).

Previous findings of increased pedestrian-level wind speed provided by a ventilation corridor mainly focused on situations in which the corridor's orientation matched the prevailing wind direction. In this study, although the corridor's axis was perpendicular to the prevailing wind direction, the pedestrian-level wind environment within the inner urbanised area still improved. This may relate to the corridor's orientation facing the waterfront, which allowed sea breezes to penetrate more easily, further influencing the ventilation performance of the entire area regardless of street orientation. This suggests that ventilation corridors along waterfronts have the potential to allow winds to penetrate inner urbanised area even when the prevailing winds do not match the corridor's axis.

Along the waterfront, the green belt's proximity to the sea showed the potential to cool the downwind area during daytime, with a mean T_a reduction of 0.1 °C. This differed from previous reports that turf had no significant cooling effect (Cheung and Jim, 2019) and could even lead to a higher T_a along a lake (Shi et al., 2020). However, Fung and Jim (2020) monitored one lawn plot situated downwind of a pond bank and found that the pondside lawn registered the lowest T_a. We believe that these conflicting results might be caused by differences in wind speed and direction relative to the water body, the size of the water body, and the distance between the water body and green infrastructure. For example, green belts downwind of the sea may experience higher cooling potential than areas near ponds, lakes, or rivers. Our finding that green roofs and green facades had the greatest impact on exterior T_s reduction was in accordance with earlier studies in Hong Kong (Cheung and Jim, 2019; Fung and Jim, 2020). Compared with the shading effect of high-rise buildings, street greenery and green roofs did not play a significant role in reducing the street average T_a, similar to previous studies findings that insufficient green coverage ratio for street greenery (Ng et al., 2012) and installation of green roofs (irrespective of type) in medium- and high-density neighbourhoods had negligible effects on pedestrian cooling (Chen et al., 2009). However, the green facade showed a slight diurnal cooling potential for street level (Salisbury Road) averaged T_a, as corroborated by a study in Hong Kong showing that benefits at pedestrian height were enhanced when vertical greening facilities were placed along a podium (Morakinyo et al., 2019). Moreover, cooling intensity was extended 50 m further north by a green facade along the waterfront, compared with a previous study's finding of about 20 m from a lake border with forest. This finding expands the existing knowledge of the synergistic cooling effects of green facades and seashores, indicating that green facades along waterfronts have the potential to extend the cooling area in inner urbanised areas.

4.2. Practical implication for UHI mitigation strategies along waterfronts

Although separate UHI mitigation strategies for redeveloped building forms, ventilation corridors, and extensive greenery along waterfronts may have opposing or negligible effects, their synergistic effects show the potential for improvements in microclimate and thermal comfort for both waterfronts and inner urbanised areas. Thus, bioclimatic design in such settings is of great importance, and a calibrated combination of mitigation strategies should be used based on the climate and urban context. We suggest that a combination of redeveloped high-rise buildings connected with a ventilation corridor along the waterfront would result in a more acceptable pedestrian-level wind environment in leeward areas and enhance the wind permeability into inner urbanised areas. This is because high-rise buildings can block the strong prevailing winds from the water, while the ventilation corridor offsets part of the V_a decrease caused by the high-rise within the inner urbanised area. Our ventilation corridor findings are consistent with some SBD guidelines, which suggest building permeability/gaps as well as intervening spaces, to permit air flow to penetrate more deeply into streets. Green belt proximity to the sea is recommended as it shows a slight cooling potential in downwind areas. In addition, green facades along the waterfront can not only cool down surrounding streets, but also extend the cooling zone within the inner urbanised area. The waterfront green facade findings are especially significant as they expand our existing knowledge of the synergistic cooling effects of green facades and waterbodies. Thus, considering the limited space available for tree planting in Hong Kong, green facades at waterfronts should be taken into consideration to optimise the cooling potential in street canyons.

5. Conclusions

We evaluated the synergistic effect of UHI mitigation strategies on local microclimate and outdoor thermal comfort in a waterfront and inner urbanised setting of Hong Kong's Victoria Dockside area. Three scenarios for a typical summer day were simulate using ENVI-met: the pre-existing configuration (Case A), a redeveloped building form (Case B), and Case B with added ventilation corridor and extensive greenery (Case C). Although the synergistic effects of building form, ventilation corridors, and extensive greenery do not combine in a linear fashion, the microclimate and thermal comfort in both settings showed overall improvement through their application. The combination of high-rise buildings and ventilation corridors along the waterfront can result in a better pedestrian-level wind environment within inner urbanised areas, despite the fact that standalone high-rise buildings may lead to relatively worse surrounding wind environments.

In addition, ventilation corridors along waterfronts can allow airflow to penetrate inner urbanised areas even when prevailing winds do not match the corridor's axis. Moreover, the proximity of turf to the sea has a slight potential to cool downwind areas during the daytime, while green facades can extend the cooling intensity 50 m further. This verifies the significance of appropriate greenery use to expand the cooling potential in such areas. Our results demonstrate the synergistic effects of bioclimatic design on UHI mitigation along waterfronts.

6. References

Adams LW, Dove LE, 1989. Wildlife reserves and corridors in the urban environment. A guide to ecological landscape planning and resource conservation. Washington, DC: National Institute for Urban Wildlife.

An K, Wong SM, Fung JCH, 2018. Exploration of sustainable building morphologies for effective passive pollutant dispersion within compact urban environments. Building and Environment 148: 508-523.

Arnfield AJ, 2003. Two decades of urban climate research: a review of turbulence, exchanges of energy and water, and the urban heat island. International Journal of Climatology 23: 1-26.

Battista G, Carnielo E, Vollaro RDL, 2016. Thermal impact of a redeveloped area on localized urban microclimate: A case study in Rome. Energy and Buildings 133: 446-454.

Bruse M, Fleer H, 1998. Simulating surface-plant-air interactions inside urban environments with a three-dimensional numerical model. Environmental Modelling and Software 13: 373-384.

Chan EHW, Yung EHK, 2004. Is the development control legal framework conducive to a sustainable dense urban development in Hong Kong? Habitat International 28(3): 409-426.

Chen H, Ooka R, Huang H, Tsuchiya T, 2009. Study on mitigation measures for outdoor thermal environment on present urban blocks in Tokyo using coupled simulation. Building and Environment 44(11): 2290-2299.

Cheng L, Guan D, Zhou L, Zhao Z, Zhou J, 2019. Urban cooling island effect of main river on a landscape scale in Chongqing, China. Sustainable Cities and Society 47: 101501.

Cheng V, Ng E, 2006. Thermal comfort in urban open spaces for Hong Kong. Architectural Science Review 49(3): 236-242.

Cheung PK, Jim CY, 2018. Comparing the cooling effects of a tree and a concrete shelter using PET and UTCI. Building and Environment 130: 49-61.

Cheung PK, Jim CY, 2019. Effects of urban and landscape elements on air temperature in a high-density subtropical city. Building and Environment 164: 106362.

Davtalab J, Deyhimi SP, Dessi V, Hafezi MR, Adib M, 2020. The impact of green space structure on physiological equivalent temperature index in open space. Urban Climate 31: 100574.

De Jesus MP, Lourenço JM, Arce RM, Macias M, 2017. Green façades and in situ measurements of outdoor building thermal behaviour. Building and Environment 119: 11-19.

Du Y, Mak CM, Tang B, 2018. Effects of building height and porosity on pedestrian level wind comfort in a high-density urban built environment. Building Simulation 11: 1215-1228.

Elnahas M, 2003. The effects of urban configuration on urban air temperatures. Architectural Science Review 46: 135-138.

Fan M, Chau CK, Chan EHW, Jia J, 2017. A decision support tool for evaluating the air quality and wind comfort induced by different opening configurations for buildings in canyons. Science of the Total Environment 574: 569-582.

Fung CKW, Jim CY, 2020. Influence of blue infrastructure on lawn thermal microclimate in a subtropical green space. Sustainable Cities and Society 52: 101858.

Giannopoulou K, Santamouris M, Livada I, Georgakis C, Caouris Y, 2010. The impact of canyon geometry on intra-urban and urban: Suburban night temperature differences under warm weather conditions. Pure and Applied Geophysics 167: 1433-1449.

Hathway EA, Sharples S, 2012. The interaction of rivers and urban form in mitigating the Urban Heat Island effect: A UK case study. Building and Environment 58: 14-22.

He BJ, Ding L, Prasad D, 2020. Relationships among local-scale urban morphology, urban ventilation, urban heat island and outdoor thermal comfort under sea breeze influence. Sustainable Cities and Society 60: 102289.

Hoelscher MT, Nehls T, Jänicke B, Wessolek G, 2016. Quantifying cooling effects of façade greening: Shading, transpiration and insulation. Energy and Buildings 114: 283-290.

Hong Kong Observatory, 2020. Number of Very Hot days and Hot Nights. Available at: https://www.hko.gov.hk/en/cis/statistic/vhotday_statistic.htm.

IPCC, 2018. Summary for Policymakers. In: Global Warming of 1.5°C. An IPCC Special Report on the impacts of global warming of 1.5°C above pre-industrial levels and related global greenhouse gas emission pathways, in the context of strengthening the global response to the threat of climate change, sustainable development, and efforts to eradicate poverty.

Johansson E, Emmanuel R, 2006. The influence of urban design on outdoor thermal comfort in the hot, humid city of Colombo, Sri Lanka. International Journal of Biometeorology 51: 119-133.

Karakounos I, Dimoudi A, Zoras S, 2018. The influence of bioclimatic urban redevelopment on outdoor thermal comfort. Energy and Buildings 158: 1266-1274.

Klemm W, Heusinkveld BG, Lenzholzer S, Hove B, 2015. Street greenery and its physical and psychological impact on thermal comfort. Landscape and Urban Planning 138: 87-98.

Kong F, Sun C, Liu F, Yin H, Jiang F, Pu Y, Cavan G, Skelhorn C, Middel A, Dronova I, 2016, Energy saving potential of fragmented green spaces due to their temperature regulating ecosystem services in the summer. Applied Energy 183: 1428-1440.

Kwok YT, Schoetter R, Lau KKL, Hidalgo J, Ren C, Pigeon G, Masson V, 2019. How well does the Local Climate Zone scheme discern the thermal environment of Toulouse (France)? An analysis using numerical simulation data. International Journal of Climatology 39(14): 5292-5315.

Lai A, Maing M, Ng E, 2017. Observational studies of mean radiant temperature across different outfoot spaces under shaded conditions in densely built environment. Building and Environment 114: 397-409.

Lan Y, Zhan Q, 2017. How do urban buildings impact summer air temperature? The effects of building configurations in space and time. Building and Environment 125: 88-98.

Lau KKL, Ren C, Ho J, Ng E, 2016. Numerical modelling of mean radiant temperature in high-density sub-tropical urban environment. Energy and Buildings 114: 80-86.

Lensky IM, Mindali OR, Michael Y, Helman D, 2015. The role of local land-use on the urban heat island effect of Tel Aviv as assessed from satellite remote sensing. Applied Geography 56: 145-153.

Lin TP, Tasi KT, Liao CC, Huang YC, 2013. Effects of thermal comfort and adaptation on park attendance regarding different shading levels and activity types. Building and Environment 59: 599-611.

Liu K, Hsueh S, Wu W, Chen Y, 2012. A Fuzzy-DAHP decision-making model for evaluating energy-saving design strategies for residential buildings. Energies 5: 4462-4480.

Lobaccaro G, Acero JA, 2015. Comparative analysis of green actions to improve outdoor thermal comfort inside typical unban street canyons. Urban Climate 14(2): 251-267.

Morakinyo TE, Lai A, Lau KKL, Ng E, 2019. Thermal benefits of vertical greening in a high-density city: Case study of Hong Kong. Urban Forestry & Urban Greening 37: 42-55.

Morakinyo TE, Kong L, Lau KKL, Yuan C, Ng E, 2017. A study on the impact of shadow-cast and tree species on in-canyon and neighborhood's thermal comfort. Building and Environment 115: 1-17.

Ng E, 2009. Policies and technical guidelines for urban planning of high-density cities – air ventilation assessment (AVA) of Hong Kong. Building and Environment 44: 1478-1488.

Ng E, Yuan C, Chen L, Ren C, Fung JCH, 2011. Improving the wind environment in high-density cities by understanding urban morphology and surface roughness: A study in Hong Kong. Landscape and Urban Planning 101: 59-74.

Ng E, Chen L, Wang Y, Yuan C, 2012. A study on the cooling effects of greening in a high-density city: An experience from Hong Kong. Building and Environment 47: 256-271.

Oke TR, 1981. Canyon geometry and the nocturnal urban heat island: Comparison of scale model and field observations. Journal of Climate 1(3): 237-254.

Oke TR, 1982. The energetic basis of the urban heat island. Quarterly Journal of Royal Meteorological Society 108: 1-24.

Ouyang W, Morakinyo TE, Ren C, Ng E, 2020. The cooling efficiency of variable greenery coverage ratios in different urban densities: A study in a subtropical climate. Building and Environment 174: 106772.

Planning Department, 2005. Feasibility study for establishment of air ventilation assessment system – final report. Planning Department, Hong Kong SAR Government.

Shi D, Song J, Huang J, Zhuang C, Guo R, Gao Y, 2020. Synergistic cooling effects (SCEs) of urban green-blue spaces on local thermal environment: A case study in Chongqing, China. Sustainable Cities and Society 55: 102065.

Siu LW, Hart MA, 2013. Quantifying urban heat island intensity in Hong Kong SAR, China. Environmental Monitoring and Assessment 185(5): 4383-4398.

Sternberg T, Viles H, Cathersides A, 2011. Evaluating the role of ivy (Hedera helix) in moderating wall surface microclimates and contributing to bioprotection of historic buildings. Building and Environment 46: 293-297.

Svensson MK, 2004. Sky view factor analysis – implications for urban air temperature differences. Meteorological Applications 11: 201-211.

Takebayashi H, Moriyama M, 2012. Relationships between the properties of an urban street canyon and its radiant environment: Introduction of appropriate urban heat island mitigation technologies. Solar Energy 86(9): 2255-2262.

Tan Z, Lau KKL, Ng E, 2016. Urban tree design approaches for mitigating daytime urban heat island effect in a high-density urban environment. Energy and Buildings 114: 265-274.

Thorsson S, Lindberg F, Eliasson I, Holmer B, 2007. Different methods for estimating the mean radiant temperature in an outdoor urban setting. International Journal of Climatology 27: 1983-1993.

Tuller SE, 1995. Onshore flow in an urban area: microclimatic effects. International Journal of Climatology 15: 1387-1398.

Unger J, 2009. Connection between urban heat island and sky view factor approximated by a software tool on a 3D urban database. International Journal of Environment and Pollution 36: 59-80.

Wang Y, Berardi U, Akbari H, 2016. Comparing the effects of urban heat island mitigation strategies for Toronto, Canada. Energy and Buildings 114: 2-19.

Wong NH, Chen Y, Ong CL, Sia A, 2003. Investigation of thermal benefits of rooftop garden in the tropical environment. Building and Environment 38(2): 261-270.

Wong NH, Tan AYK, Chen Y, Sekar K, Tan PY, Chan D, Chiang K, Wong NC, 2010. Thermal evaluation of vertical greenery systems for building walls. Building and Environment 45(3): 663-672.

Xu J, Wei Q, Huang X, Zhu X, Li G, 2010. Evaluation of human thermal comfort near urban waterbody during summer. Building and Environment 45: 1072-1080.

Yang F, Lau SSY, Qian F, 2011. Urban design to lower summertime outdoor temperatures: An empirical study on high-rise housing in Shanghai. Building and Environment 46: 769-785.

Yin C, Yuan M, Lu Y, Huang Y, Liu Y, 2018. Effects of urban form on the urban heat island effect based on spatial regression model. Science of the Total Environment 634: 696-704.

Yuan C, Ng E, 2012. Building porosity for better urban ventilation in high-density cities—A computational parametric study. Building and Environment 50: 176-189.